ELSEVIER

Journal of Nuclear Materials 266–269 (1999) 182–188

journal of nuclear materials

Role of divertor geometry on detachment and core plasma performance in JT60U

N. Asakura *, N. Hosogane, K. Itami, A. Sakasai, S. Sakurai, K. Shimizu, M. Shimada, H. Kubo, S. Higashijma, H. Takenaga, H. Tamai, S. Konoshima, T. Sugie, K. Masaki, Y. Koide, O. Naito, H. Shirai, T. Takizuka, T. Ishijima, S. Suzuki, A. Kumagai, JT-60 Team

Naka Fusion Research Establishment, Japan Atomic Energy Research Institute, Naka-machi, Naka-gun Ibaraki-ken, 311-01, Japan

Abstract

Experimental results related to the divertor geometry such as divertor plasma detachment, neutral transport and plasma energy confinement, were compared in the open and W-shaped divertors. The ion flux near the outer strike point was larger than in the open divertor, and the electron temperature at the target, T_e^{div}, was reduced. Divertor detachment and x-point MARFEs occurred at $\bar{n}_e$ 10–20% lower than that for the open divertor. Although the leakage of neutrals from the divertor to the main chamber decreased, a neutral source in the main chamber due to an interaction of the outer scrape-off layer (SOL) plasma to the baffle plates became dominant above the baffle. Degradation in the enhancement factor of the energy confinement was observed similarly in the open and W-shaped divertors. The neutral density inside the separatrix was estimated to be a factor of 2–3 smaller, which did not affect the energy confinement.

Keywords: Divertor; Divertor plasma; Detached plasma; Neutral transport; Energy confinement time

1. Introduction

Experimental campaigns using a new semi-closed W-shaped divertor have been carried out in long pulse (5–9 s) ELMy H-mode plasmas on JT-60U. The principal goal is demonstration of a cold-and-dense or detached divertor plasma with sufficient enhancement of the energy confinement for ITER R & D design. Control of the dense neutrals in the divertor chamber and reduction in neutral backflow to the main chamber is required. The divertor geometry was designed to control recycling neutrals [1] with an exhaust system using the neutral beam injector cryo-pump units. In order to increase the neutral density at the strike point, the inner and outer divertor targets are inclined at angles of 70 and 60 degrees, respectively. They are joined to baffle plates at the divertor throat in order to minimize a leakage of recycling neutrals from the divertor chamber. A private dome separates neutral transport between the inner and outer divertors in order to improve the pumping efficiency from the inner private region. In this paper, conditions for the detachment of the divertor plasma, particle recycling, and energy confinement of the core plasma are compared for the W-shaped divertor and the previous open divertor on JT-60U.

A database of high plasma current ($I_p = 1.7$ MA), NB-heated L-mode (injected power of neutral beam, $P_{NBI} = 4.1$–4.3 MW) discharges was used for the divertor and SOL plasma study. Plasma parameters for the W-shaped divertor such as I_p, plasma volume ($V_p = 77$ m^3) and triangularity ($\delta = 0.32$) were slightly different from those for the open divertor [2] (1.8 MA, 82 m^3 and 0.24, respectively). The toroidal field ($B_T = 3.5$ T), safety factor ($q_{95} = 3.4$–3.6), major and minor radii at midplane ($R = 3.43$–3.46 m and $a_{mid} = 0.95$–0.98 m), and elongation ($\kappa = 1.4$) are the same for the two cases. Another

* Corresponding author. Tel.: +81-29 270 7613; fax: +81-29 270 7339; e-mail: asakuran@naka.jaeri.go.jp

0022-3115/99/$ – see front matter
PII: S0022-3115(98)00818-6

database of the low plasma current ($I_p = 1.0$–1.2 MA, $B_T = 2.1$–2.7 T and $q_{95} = 3.4$–3.7) NB-heated ELMy H-mode ($P_{NBI} = 16$–21 MW) discharges was used for study of core plasma confinement and neutral recycling. For reducing the toroidal ripple loss of the fast ions, plasma configuration parameters such as $V_p = 57$–64 m^3, $R = 3.24$–3.30 m, $a_{mid} = 0.82$–0.86 m and $\delta = 0.17$–0.20 were smaller than those used in the L-mode plasmas.

2. Divertor plasma and detachment

The effect of the divertor geometry on the divertor plasma was investigated. Plasma profiles at the divertor target were measured with a Langmuir probe array illustrated in Fig. 1(a). A comparison of profiles of electron density, n_e^{div}, and temperature, T_e^{div}, at the outer divertor target is shown in Fig. 1(b) and (c). These were measured at relatively high $\bar{n}_e$ (2.4×10^{19} m^{-3} for closed symbols, and 2.8×10^{19} m^{-3} for open symbols). At the same $\bar{n}_e$, the electron density measured with a midplane

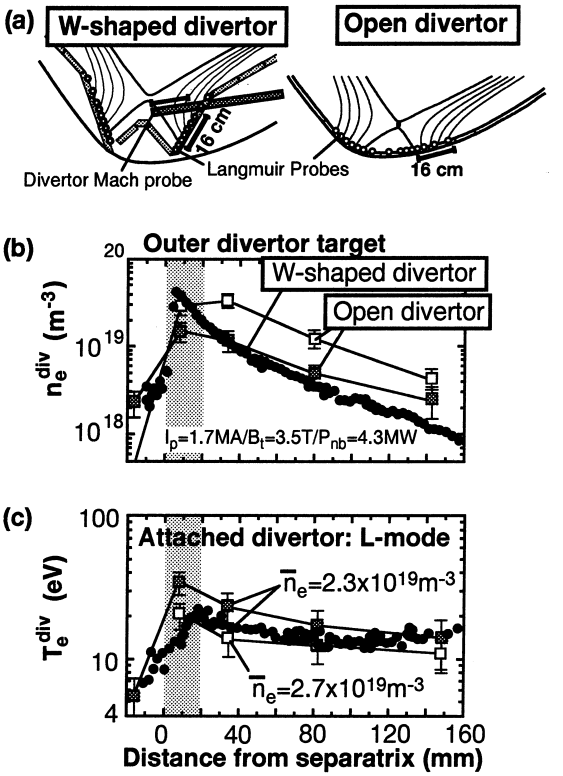

Fig. 1. (a) Divertor geometry of the open and the W-shaped divertors. Locations of target Langmuir probes and scanning chord of a reciprocating probe are shown. (b) electron density, (c) temperature profiles at the outer divertor target. Circle and square symbols show the open and W-shaped divertors. Profile for the W-shaped divertor is measured during x-point sweep.

reciprocating probe, n_e^{mid}, was 1.5×10^{19} m^{-3} for the W-shaped divertor, which was slightly higher than that for the open divertor (1.3×10^{19} m^{-3}). A large peak in the n_e^{div} profile is observed near the strike point in the W-shaped divertor. The peak profile can be measured with a spatial resolution of a few mm during a plasma x-point sweep (the x-point height from the dome top was varied from 8 to 14 cm in 1.5 s) while keeping the same V_p and $\bar{n}_e$. A large peak in the n_e^{div} profile (larger than an e-folding slope) has not been observed at the outer strike point in the open divertor [3].

For the W-shaped divertor, n_e^{div} near the strike point is enhanced by a factor of 2, and the local T_e^{div} decreases to 14 eV. However, the total ion flux flowing to the outer divertor target was 20–30% higher than that for the open divertor. These results indicate that the inclined divertor target and the private dome are effective in condensing neutrals near the separatrix rather than increase the total particle recycling in the divertor chamber.

Divertor plasma detachment occurred at the outer strike point when the radiation power was enhanced in the vicinity of the x-point. The radiation power near the x-point was enhanced substantially due to an increase in radiation from carbon ions (C^{3+}). This increase in radiation defines the onset of the 'x-point MARFE'. The transition to the x-point MARFE, was similar to that in the open divertor [4]. The time evolution of the electron temperature, T_e^{xp}, and electron pressure, p_e^{xp}, near the x-point (just downstream) were measured with an x-point reciprocating probe [5] [scanning chord is illustrated in Fig. 1(a)]. These profiles and the location of detachment upstream from the target plate are shown in Fig. 2(a) and (b). Under the attached divertor condition, T_e^{xp} decreases to 10–20 eV near the strike point with an increase in the local electron density (1.2×10^{20} m^{-3}), while the electron temperature at the midplane is 70 eV. This result shows that the temperature decreases largely at or above the x-point rather than in the divertor chamber.

During the x-point MARFE, T_e^{xp} decreases to $\sim$5 eV, and p_e^{xp} is reduced to 13 Pa, while the electron pressure at the midplane, p_e^{mid}, is 130 Pa. The radial width of the region of low T_e^{xp} is about 3.5 cm. Fig. 2(c), shows that a reduction in p_e^{div} is observed at the same magnetic surface ($\leqslant 2$ cm at the outer target). The value of T_e^{div} in the region of detachment was about $\sim$5 eV, which is lower than that for the open divertor (8–10 eV). The detached region is represented by hatched area. Divertor plasma detachment occurs simultaneously at all points along the field line, and at the same time, in the outer flux surfaces the T_e^{xp} profile becomes flat and n_e^{xp} increases. Radial diffusion of particle flux may be enhanced upstream from the x-point. The large peak in the p_e^{xp} profile, ($= 300$ Pa, which is larger than p_e^{mid} of 130–200 Pa) shifts to the boundary of the attached flux region. A similar transition was observed in ASDEX-Upgrade [6]. The pressure loss factor, p_e^{mid}/p_e^{xp}, is evaluated to be 10

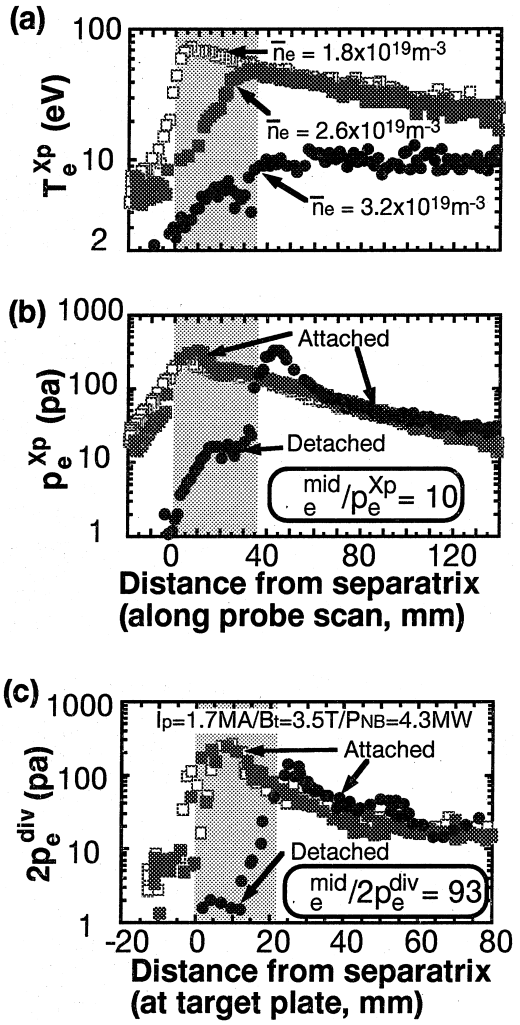

Fig. 2. Profiles of (a) electron temperature, (b) electron pressure near x-point and (c) at the outer target. Square and circle symbols show the attached and detached divertor plasma. Hatched area shows the region, where the plasma is detached.

(= 130/13) below the x-point, and $p_e^{mid}/2p_e^{div}$ = 93 (= 130/1.4) at the outer target. The latter value is larger than $p_e^{mid}/2p_e^{div} \leqslant 20$ for the open divertor. Due to the lower T_e^{div} and larger neutral density, elastic and charge-exchange collisions increase near the target.

Fig. 3 shows the onset density of the divertor detachment, n_e^{onset}, normalized by the 'Greenwald density', $n^{Gr} \equiv I_p/\pi a_{mid}^2$ [MA m^{-2}], as a function of the net input power, P_{net}. The database is obtained in all ELMy H-mode discharges except for those with low P_{net}. Values of n_e^{onset} for the W-shaped divertor range between 0.50–0.65, which are 10–20% lower than those for the open divertor [7] (0.67–0.75). The large scatter in n_e^{onset} is caused mainly by gas puffing locations: n_e^{onset} for puffing at the main chamber is systematically higher than n_e^{onset}

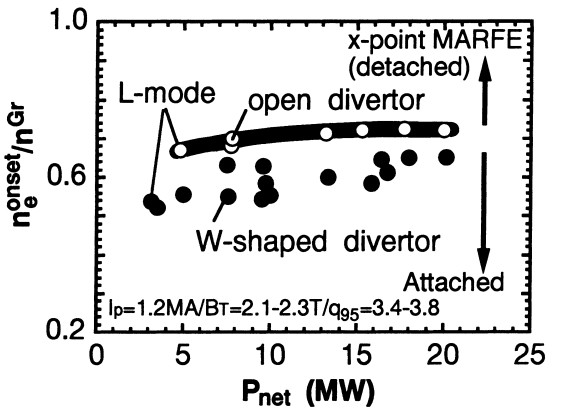

Fig. 3. Onset density of the divertor detachment, neonset, normalized by 'Greenwald density', n^{Gr}, as a function of the net input power, P_{net}. Open and closed symbols show the open and W-shaped divertors. Database is for low safety factor ($q_{95} = 3.4$–3.7), and all ELMy H-mode except for low P_{net}.

for private-region puffing. The divertor radiation fraction (P_{rad}^{div}/P_{sol}, where $P_{sol} = P_{abs} - P_{rad}^{main}$, P_{abs} plasma absorbed power and P_{rad}^{main} is radiation loss at the main plasma) was 0.35–0.45 at n_e^{onset}, which was the same level as for the open divertor. The concentration of the carbon ions in the vicinity of the x-point was not decreased, although the impurity influx due to chemical sputtering was reduced [8].

3. Control of recycling neutrals

3.1. Control efficiency of recycling neutrals

The efficiency of controlling recycling neutrals ('neutral compression') in the divertor device is represented by the ratio of neutral density at the divertor, n_0^{div}, to that in the main chamber, n_0^{main}. The brightness of the D_α line is approximately proportional to the local neutral and electron densities, and changes in the neutral density between the open and W-shaped divertors can be compared.

Neutral ionization fluxes at the main plasma edge and divertor, $\Phi_{D_\alpha}^{main}$ and $\Phi_{D_\alpha}^{div}$, are deduced by integrating the D_α signals [3] viewing the upper main plasma (channels 1–3) and divertor (channels 6–10), respectively. The viewing chords are shown in Fig. 4(a). Under an attached divertor condition, an increase in $\Phi_{D_\alpha}^{div}$ with $\bar{n}_e$ (from 2×10^{22} to (3–5) $\times 10^{23}$ s^{-1}) is similar for the W-shaped and open divertors. The value of $\Phi_{D_\alpha}^{main}$ also increases with $\bar{n}_e$, but $\Phi_{D_\alpha}^{main}$ for the W-shaped divertor is a factor of 2–3 smaller than that for the open divertor. The efficiency of controling recycling neutral is improved for the W-shaped divertor. For the W-shaped divertor, the in-vessel neutral pressure near the entrance

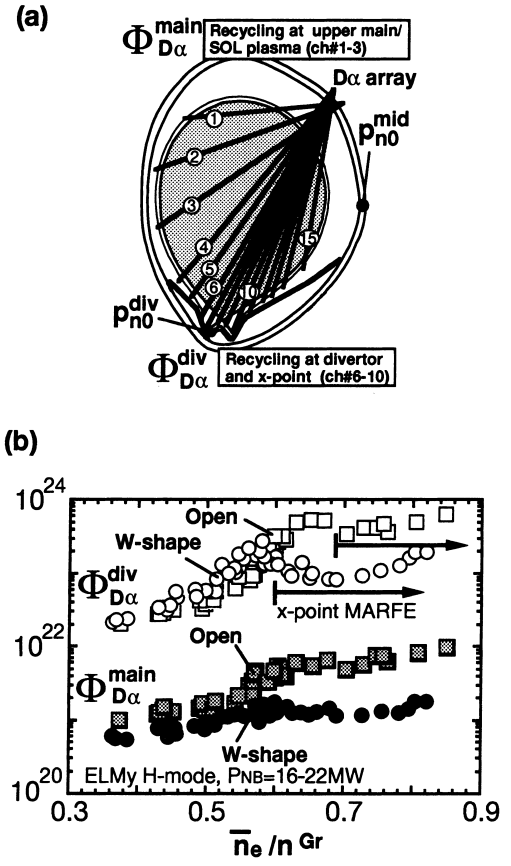

Fig. 4. (a) Sightlines of 15-channel D_α brightness measurement, and ASDEX-type neutral gas pressure analyzers. (b) neutral ionization fluxes at the main plasma edge and divertor, $\Phi_{D\alpha}^{main}$(open symbols) and $\Phi_{D\alpha}^{div}$ (closed symbols), are deduced from D_α signals. Square and circle symbols show the open and W-shaped divertors.

of the exhaust slot at the inner private region, $p_{n_0}^{div}$, and that at the outer midplane, $p_{n_0}^{div}$, were measured with ASDEX-type neutral analyzers [9]. In similar ELMy H-mode discharges, value of $p_{n_0}^{div}$ increased from 0.1 to 1.5 Pa, while $p_{n_0}^{div}$ increased from 0.2 to 1.2 mPa for the W-shaped divertor. The maximum neutral compression was about 1000.

3.2. Neutral source distribution

Particle recycling is generally the most important contribution in fuelling the main plasma. A change in the divertor geometry affects the distributions of neutral sources and neutral density. These parameters have been investigated by the Monte Carlo method with a two-dimensional neutral transport code [10]. The plasma density and temperature distributions in the SOL region are determined by solving the one-dimensional fluid equations based on measured T_e^{div} and n_e^{div} profiles. The model fairly well describes the measured T_e, T_i and n_e at the main plasma edge under attached divertor conditions. Neutrals are produced largely at the divertor target, and the flux is expressed as $\Phi_{n_0}^{div}$. Other neutral sources are desorption from the first wall (and from the baffle plates for the W-shaped divertor), gas puffing, and the energetic neutral beam injection. Those fluxes are denoted as $\Phi_{n_0}^{wall}$ and $\Phi_{n_0}^{baffle}$, $\Phi_{n_0}^{puff}$ and $\Phi_{n_0}^{NBI}$, respectively.

To validate the neutral distribution, a comparison between calculated D_α brightness profiles (circle and triangle symbols represent those for divertor and wall/baffle sources) and the measured one (square symbols) is shown in Fig. 5(b) and (c). Here, the D_α brightness profile is reconstructed by integrating $\langle\sigma v\rangle n_0 n_e$ along the

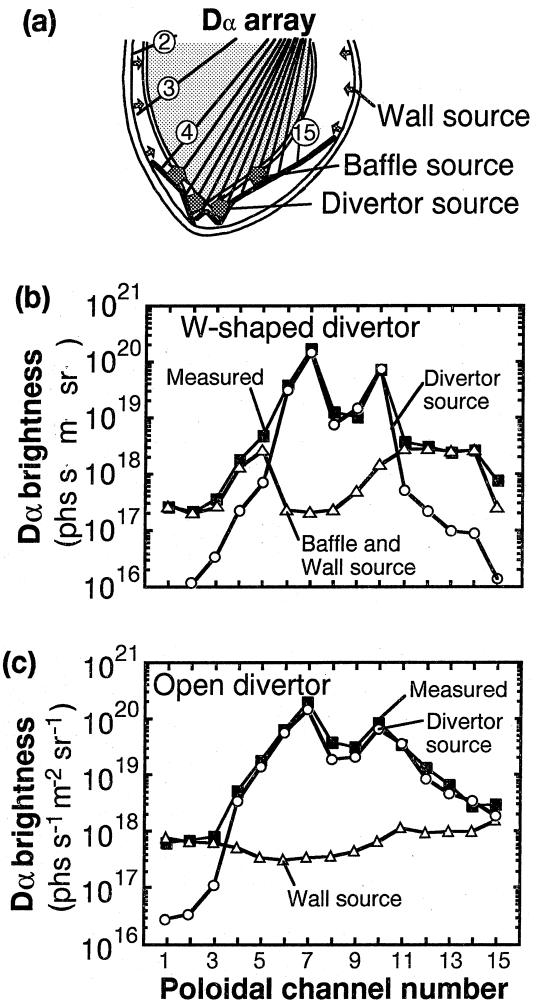

Fig. 5. (a) Source locations are illustrated for the W-shaped divertor, and viewing chords. (b) D_α brightness profiles for the W-shaped divertor, and (c) for the open divertor. Reconstructed D_α brightness profile: circle and triangle symbols for divertor and wall/baffle sources, and measured one (squares).

viewing chords as shown in Fig. 5(a), where n_0 and n_e are calculated neutral and electron densities, and $\langle\sigma v\rangle$ is the photon emission rate coefficient for neutral ionization [11]. For the open divertor the calculated and measured D_α brightness profiles agree well at the main plasma below the midplane and in the divertor. For explaining the measured D_α brightness at the upper main plasma, an additional neutral source, $\Phi_{n_0}^{\rm wall}$ of 8×10^{21} s^{-1}, is introduced in the model. The value of $\Phi_{n_0}^{\rm wall}$ increases from 1×10^{21} to 2×10^{22} s^{-1} as $\bar{n}_e$ is increased from 2.1×10^{19} to 3.2×10^{19} m^{-3}. These values correspond to 2.4–4% fo $\Phi_{n_0}^{\rm div}$.

For the W-shaped divertor, the calculated and measured D_α brightness profiles agree well in the divertor. Above the baffle plates, the calculated D_α brightness due to the divertor source decreases significantly: leakage of neutrals from the divertor to the main chamber is small. On the other hand, the measured D_α brightness profile near the baffle plates is an order of magnitude larger than the calculated value. Additional neutral sources from the first wall, inner and outer baffle plates, $\Phi_{n_0}^{\rm wall}$, $\Phi_{n_0}^{\rm baffle,in}$ and $\Phi_{n_0}^{\rm baffle,out} = 6 \times 10^{20}$, 3×10^{21} and 5×10^{21} s^{-1}, respectively, are introduced. Above the baffle plates, the penetration probability of neutrals through the SOL (26%) is larger than that at the divertor (1.8%). The penetration probability of the baffle source is larger than that of the wall source by a factor of 1.4, since the distance from the separatrix to the baffle plate is smaller than that to the first wall. The ionization source inside the separatrix originating from the baffle plates and the first wall, $S^{\rm baffle/wall}$, is 2.2×10^{21} s^{-1}, which is still smaller than that from divertor source, $S^{\rm div} = 5.5 \times 10^{21}$ s^{-1}. However, $S^{\rm baffle/wall}$ becomes a larger contribution to fuelling inside the separatrix (40%), comparing to the wall source for the open divertor (15–20%).

For the W-shaped divertor with pumping, a factor of 2–6 larger gas puff rate ($\Phi_{n_0}^{\rm puff} = (1\text{–}3) \times 10^{22}$ s^{-1}) is required than for the open divertor in order to maintain high density in the main plasma. This is particularly true for high power ELMy H-mode plasmas. The total ionization inside the separatrix from $\Phi_{n_0}^{\rm div}$, $\Phi_{n_0}^{\rm wall}$ and $\Phi_{n_0}^{\rm baffle}$ is 7.7×10^{21} s^{-1}, which is a factor of 2 smaller than that for the open divertor. Here, in this case $\Phi_{n_0}^{\rm NBI} = 1.1 \times 10^{21}$ s^{-1} (fuelling directly inside separatrix) is small. The time-averaged $\Phi_{n_0}^{\rm puff} = 1.8 \times 10^{22}$ s^{-1} (25 Pa m^3 s^{-1}), and the ionization flux inside the separatrix is 4×10^{21} s^{-1}. Due to mechanical limitation, more effective fuelling methods such as the pellet injector are required for the high density operation.

3.3. Neutral source at baffle plates

The leakage of neutrals from the exhaust path (under the baffle plates) was designed to be less than 1×10^{21} molecules/s, which is smaller than the total $\Phi_{n_0}^{\rm baffle}$ of 8×10^{21} s^{-1}. Two (i.e. first and second) SOL regions with different characteristic lengths are measured in the $n_e^{\rm mid}$ profile with a midplane reciprocating probe as shown in Fig. 6(a). The outer SOL region (second SOL) with 3–4 times larger than the *e*-folding length near the separatrix extends to the first wall. This was similar both before [2] and after installation of the baffle plate. The particle flux to the outer baffle plates is estimated by integrating the profile of ion flux density between 4 and 10 cm from the separatrix at the midplane, which is defined as $\Phi_{\rm probe}^{\rm mid}$. Toroidal symmetry in the ion flux profile is assumed. A comparison between the particle flux and the neutral ionization fluxes above the outer baffle, $\Phi_{D_\alpha}^{\rm baffle,out}$, is shown in Fig. 6(b). The value of $\Phi_{D_\alpha}^{\rm baffle,out}$ is deduced from integrating the D_α signals for chords viewing the outer main plasma (channels 11–15), where the ionization of neutrals is dominant with $T_e^{\rm mid}$ of 8–20 eV at the outer SOL. The value of $\Phi_{D_\alpha}^{\rm baffle,out}$ agrees with $\Phi_{\rm probe}^{\rm mid}$ within a factor of two, which suggests that the neutral source at the baffle plate is produced due to interaction with the outer SOL plasma. The formation

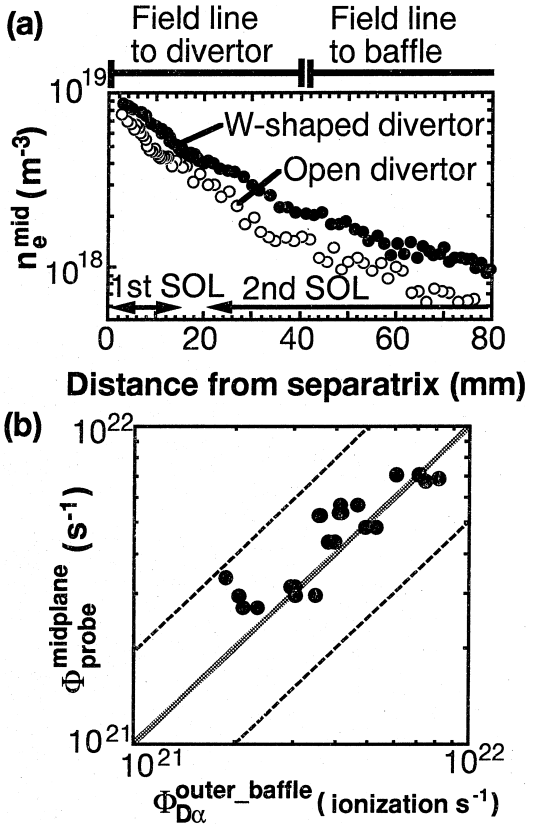

Fig. 6. (a) Electron density profiles for the open (open symbols) and the W-shaped divertor (closed symbols) at the medium denisty $\bar{n}_e = 1.8 \times 10^{19}$ m^{-3} in L-mode plasma. (b) Comparison between $\Phi_{D\alpha}^{\rm baffle,out}$ and $\Phi_{\rm probe}^{\rm mid}$ in the density scan of $\dot{n}_e = (1.1\text{–}2.7) \times 10^{19}$ m^{-3}.

mechanism of the second SOL such as diffusion, neutral ionization from the first wall or leakage from the divertor chamber has not been understood.

4. Core plasma confinement

The enhancement factor (H-factor) of the global energy confinement time has been shown to decrease with increasing neutral gas pressure in the main chamber [12–14]. This fact suggests that an increase in the neutral density inside the separatrix enhances charge-exchange loss of the ion momentum and energy at the edge transport barrier. Degradation of the H-factor and edge neutral level have been investigated for the open and W-shaped divertors. Here, the H-factor is defined as an enhancement factor of the global energy confinement time exceeding that of ITER89P L-mode scaling [15].

Fig. 7 shows the H-factor of JT-60U ELMy H-mode plasmas, with $P_{NBI} = 16$–22 MW, as a function of $\bar{n}_e/n^{Gr}$. The triangles represent the high-β_p ELMy H-mode plasmas, where the temperature and density profiles are peaked in the core plasma region [16]. The circles represent standard ELMy H-mode plasmas with a flat density profile. A high H-factor value of 1.9 is obtained at $\bar{n}_e/n^{Gr} \sim 0.5$ in the high-β_p ELMy H-mode plasmas mainly due to increasing δ up to 0.4. When the gas puffing rate is increased in order to increase the radiation loss at the divertor, the H-factor of the ELMy H-mode plasma decreases continuously from 1.8 to 1.1–1.2 under attached divertor conditions. During the x-point MARFE, the H-factor (plotted as closed circles) is further reduced to less than one. The database of ELMy H-mode plasmas for the open divertor are represented by the hatched area [7]. A similar degradation in the H-factor was observed at high density for both the open and W-shaped divertors.

The energy stored in the fast ions W_{fast} and in the thermal plasma $W_{thermal}$ are included in the global energy confinement time τ_E and the ITER89P L-mode scaling. Since W_{fast} is proportional to the slowing down time of the fast ions ($\propto T_e^{1.5}/n_e$), it decreases at high density. Fig. 7(b) shows W_{fast} thermal energy $W_{thermal}$ and the total stored energy W_{total} as a function of $\bar{n}_e$. For the W-shaped divertor, W_{total} and W_{fast} decreases from 2.4 to 1.6 MJ and from 1.0 to 0.3 MJ, respectively. $W_{thermal}$ decreases moderately from 1.3 to 1.4 MJ, and it decreases to 1.1 MJ during the x-point MARFE. The reduction of the H-factor was due to the decrease in W_{fast} and in $W_{thermal}$ with increasing $\bar{n}_e$. The increase in ELM frequency from 100 to 200 kHz at high $\bar{n}_e$ is not remarkable. The total ion plus electron pressure at the edge pedestal ($\rho = 0.95$) decreases at high $\bar{n}_e$, similar to the reduction in $W_{thermal}$. This decrease is caused by a decrease in the width of the region with large pressure gradient from $\rho = 0.95$–0.99 to 0.97–0.99, rather than

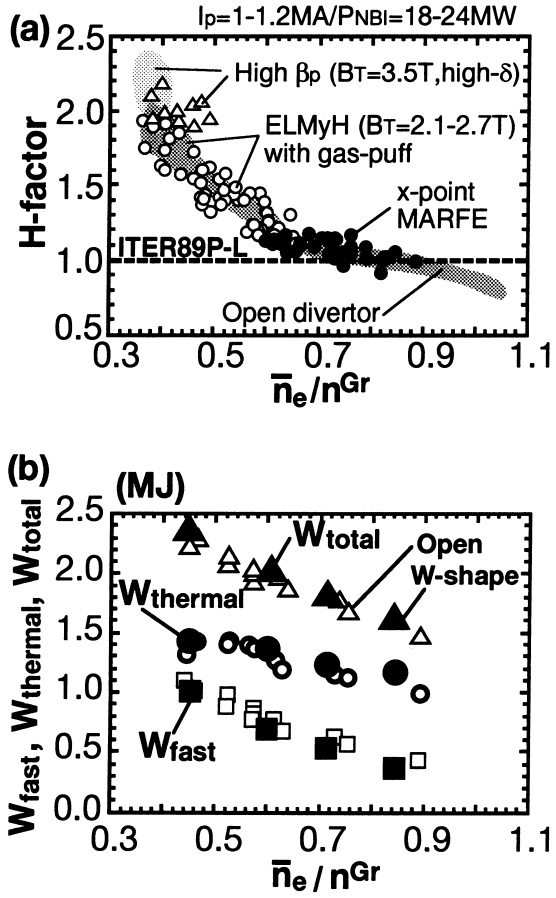

Fig. 7. H-factors based on ITER89PL-mode scaling for ELMy H-mode discharges with $P_{NBI} = 16$–22 MW as a function of n_e/n^{Gr}. Symobls and hatched area show database for the W-shaped and open divertors. (b) Total stored energy W_{total} (triangles), and energy stored in the fast ions W_{fast} (squares) and thermal plasma $W_{thermal}$ (circles).

by a reduction in the pressure gradient at the edge ($|d(n_eT_i)/d\rho| = 3.5 \times 10^4$ Pa m^{-1}).

The local neutral density inside the separatrix was estimated by the neutral transport code, and has been compared at different poloidal locations such as at the outer midplane and near the x-point, which are represented by n_0^{mid} and n_0^{xp}, respectively. These are averaged values over the cell area selected from the calculation mesh, and the minor radius of the cells is $\rho = 0.96$–1.0. When the particle recycling in the divertor is increased, n_0^{mid} increases from 6×10^{14} to 1.1×10^{15} m^{-3} for the W-shaped divertor. While n_0^{mid} is comparable at low density for the open and W-shaped divertors, n_0^{mid} at high density is a factor of 2–3 lower than for the open divertor. The value of n_0^{xp} increases from 7.2×10^{15} to 1.1×10^{16} m^{-3}, and the values are a factor of 2 smaller than those for the open divertor. As a result, the neutral density inside the

separatrix was reduced by a factor of 2–3. However, an improvement was not observed in the energy confinement, and a small reduction in H-mode threshold power of ~10% was observed [17]. A multi-machine database of n_0 and $P_{n_0}^{\mathrm{mid}}$ may determine the critical values for improvement of energy confinement. At the same time, more than half of n_0 above the baffle plates is due to desorbed neutrals from the plates rather than the back flow from the divertor. Reduction in neutral source at the baffle plates is required to maintain low neutral density.

5. Conclusion

For the W-shaped divertor, the ion flux increased near the strike point, and detachment of the divertor plasma was obtained at lower $\bar{n}_e$. The location of enhanced radiation loss (near the outer x-point) was not changed. Method of controlling impurity transport is required: pumping at outer private region is implemented for producing a SOL flow. A reduction in the neutral density at the main plasma edge by the factor of 2–3 was obtained. However, the improvement was not as good as had been predicted by design calculations [1] due to formation of an outer SOL plasma or neutral source in the main chamber. An effect of reduction in neutral density at the plasma edge on energy confinement was not clearly observed. Reduction of the neutral source in the main chamber will be required to maintain lower neutral density.

Acknowledgements

The first author would like to thank Dr K. Hill for very useful comments.

References

[1] N. Hosogane, et al., Proc. 16th Int. Conf. Montreal, 1996, vol. 3 (IAEA, Vienna, 1996) p. 555.
[2] N. Asakura, et al., J. Nucl. Mater. 241–243 (1997) 559.
[3] N. Asakura, et al., Nucl. Fusion 35 (1995) 381.
[4] N. Asakura, et al., Nucl. Fusion 37 (1996) 795.
[5] S. Sakurai, et al., these Preceedings.
[6] S. C. Pitcher, et al., J. Nucl. Mater. 220–222 (1995) 213.
[7] N. Asakura, et al., Plasma Phys. Control. Fusion 39 (1997) 1295.
[8] S. Higashijima, et al., these Preceedings.
[9] H. Tamai, et al., these Preceedings.
[10] K. Shimizu, et al., J. Nucl. Mater. 196–198 (1992) 476.
[11] L.C. Johnson, E. Hinov, J. Quant. Spectrosc. Radiat. Transfer 13 (1973) 333.
[12] S.M. Kaye, et al., J. Nucl. Mater. 212 (1984) 115.
[13] R.D. Stambaugh, et al., Plasma Phys. Control. Fusion 36 (1994) A249.
[14] The JET Team (presented by G.F. Matthews), Plasma Phys. Control. Fusion 37 (1995) A227.
[15] P.N. Yushimanov, et al., Nucl. Fusion 30 (1990) 1999.
[16] Y. Kamada, et al., Proc. 15th Int Conf. Seville, 1994, vol. 1 (IAEA, Vienna, 1995) p. 651.
[17] K. Tsuchiya, et al., Plasma Phys. Control. Fusion 40 (1998) 713.